Microstructure and chemistry of nonstoichiometric $(Ba,Sr)TiO_3$ thin films deposited by metalorganic chemical vapor deposition

Igor Levin
Ceramics Division, National Institute of Standards and Technology, Gaithersburg, Maryland 20899

Richard D. Leapman
Bioengineering and Physical Science Program, Office of Research Services, National Institutes of Health, Bethesda, Maryland 20892

Debra L. Kaiser
Ceramics Division, National Institute of Standards and Technology, Gaithersburg, Maryland 20899

(Received 27 December 1999; accepted 3 April 2000)

The microstructure and chemistry of $(Ba,Sr)TiO_3$ thin films deposited on $Pt/SiO_2/Si$ substrates by metalorganic chemical vapor deposition were studied using high-resolution transmission electron microscopy and quantitative spectrum imaging in electron energy loss spectroscopy. The grain boundaries in all films with overall Ti content ranging from 50.7% to 53.4% exhibit a significant increase in Ti/Ba ratio as compared to the grain interiors. The results suggest that the deviations of Ti/(Ba + Sr) ratio from the stoichiometric value of unity are accommodated by the creation of Ba/Sr vacancies, which segregate to the grain boundary regions. The films with Ti contents equal to or greater than 52% additionally contained an amorphous Ti-rich phase at some grain boundaries and multiple grain junctions; the amount of this phase increases with increasing overall Ti content. The analysis indicates that the amorphous phase can only partially account for the significant drop in dielectric permittivity accompanying increases in the Ti/(Ba + Sr) ratio.

Recently, much attention has been focused on the fabrication of polycrystalline thin films of barium strontium titanate (BST).[1–7] This material can offer a high dielectric permittivity at a relatively large film thickness in dynamic random-access memories,[6–8] and has properties of interest for tunable microwave devices.[7] Deposition of the BST films with an excess of Ti has been found to be necessary to achieve acceptable leakage currents and dielectric lifetimes,[9] and to obtain reproducible, stable, and smooth film morphology. However, deviation of the Ti/(Ba + Sr) ratio from the stoichiometric value of unity has an adverse effect on dielectric permittivity of the BST films.[10] For example, the dielectric constant of 40-nm-thick films decreases by about 60% when the Ti content is increased from 51 to 53.4 at.%.[10] This effect is even more pronounced for larger film thicknesses. Despite this dramatic effect of stoichiometry on the dielectric properties, the exact mechanism for accommodation of excess Ti in these films still has not been determined. Recently, structural imaging in a high-resolution transmission electron microscope (HRTEM) and high-spatial resolution electron energy loss spectroscopy (EELS) were applied to study the microstructure and chemistry of BST films deposited on $Pt/SiO_2/Si$ substrates by metalorganic chemical vapor deposition (MOCVD).[11,12] Stemmer *et al.*[11] reported a systematic increase in the Ti/O ratio at the grain boundaries of a film containing 53.4% Ti, while no such increase was detected for the specimen with 50.7% Ti. Their analysis of the energy loss near edge structure (ELNES) indicated a broadening of the Ti $L_{2,3}$ ELNES features for the 53.4% Ti specimen; this was attributed to the distortion of the oxygen octahedra due to partial accommodation of excess Ti in the lattice. Levin *et al.*,[12] working on very similar specimens, demonstrated an increase in the Ti/Ba ratio at all of the grain boundaries in a film with 53.4% Ti. They found that all of the grain boundaries in this film were Ba deficient, while some of these additionally exhibited an increase in Ti content. The latter regions were associated with an amorphous-like phase frequently observed at the grain boundaries and triple junctions in the 53.4% specimen. The amorphous phase was found to contain at least Ba, Ti, and O (no measurements of Sr content were conducted). The present contribution summarizes the results of the combined HRTEM and *quantitative* EELS analysis of the BST films with different Ti/(Ba + Sr) ratios.

The $(Ba,Sr)TiO_3$ thin films were deposited on Pt (100 nm)/SiO_2/Si substrates by high-composition precision, liquid delivery MOCVD at a substrate temperature of 640 °C.[2] Films with three different Ti contents, hereafter referred to as the 50.7%, 52% and 53.4% specimens, were studied. The average compositions of the 50.7% and the 53.4% BST films, as determined by wavelength dispersive x-ray fluorescence (XRF) spectroscopy

using well-characterized standards,[13,14] are summarized in Table I. The film thickness for all specimens was about 38 nm, as measured by XRF and subsequently confirmed by cross-sectional transmission electron microscopy (TEM).[12]

Details of the TEM specimen preparation have been given elsewhere.[12] Structural imaging was performed in a JEOL 3010UHR (300 kV) high-resolution transmission electron microscope. A VG Microscopes HB501 dedicated scanning transmission electron microscope equipped with a Gatan model 766 DigiPEELS (parallel electron energy loss spectrometer) was used for chemical analysis.[15] For this analysis, the specimen was cooled to liquid nitrogen temperature to prevent contamination. Spectrum-images (64 × 64 pixels) were recorded by scanning a focused probe of about 1.5-nm diameter over an area of about 80 × 80 nm. The thickness of the analyzed area was less than that of the BST film (38 nm). Spectra in the energy loss range from 400 to 800 eV (which includes the Ti–$L_{2,3}$, O–K, and Ba–$M_{4,5}$ edges) were acquired at each point (pixel). Specimen drift during the data acquisition was corrected by using a cross-correlation procedure implemented in the GATAN Digital Micrograph v.3. software. The spectrum-images were subsequently processed to remove the background, and maps of both the Ti–$L_{2,3}$ and the Ba–$M_{4,5}$ intensity distributions were obtained by integrating the corresponding edges over an energy window of 50 eV. The coefficient of variance due to counting statistics for the Ti/Ba ratio was about 0.01. Spectrum-imaging of the Sr–$L_{2,3}$ edge (1950 eV) was unsuccessful due to the exceedingly large acquisition times required to achieve an acceptable signal-to-noise ratio.

EELS data were quantified using single crystals of $BaTiO_3$ and $SrTiO_3$ as standards. The EELS spectra from the standards and from the BST film with 53.4% Ti were recorded during the same microscope session under similar experimental conditions. Sr and Ti were quantified by using the $L_{2,3}$ edge, and Ba by using the $M_{4,5}$ edge. Both the Ti/Ba and Ti/Sr ratios in the 53.4% film measured by EELS from 20 areas, each about 80 × 80 nm in size (Table II), agree well with those measured by XRF. Based on this result, we assumed that the average composition over the area sampled by spectrum-imaging is equal to the average composition of the entire film as measured by XRF; the maps of Ti/Ba ratio for the various films were subsequently normalized to the corresponding average values of Ti/Ba. The larger standard deviations reported for the EELS measurements reflect in part higher statistical errors associated with plural scattering and diffraction effects, as well as the background subtraction.

TEM imaging of all three films revealed similar microstructure composed of columnar grains with a mean grain diameter of about 15 nm, independent of composition. All films are fiber textured with the ⟨001⟩ direction parallel to the surface normal. No amorphous phase was detected in the 50.7% specimen, while disordered regions with amorphous-like contrast were observed occasionally at some of the multiple grain junctions in the 52% specimen (Fig. 1). In contrast, such amorphous-like regions were *frequently* observed at the grain boundaries and grain junctions in the 53.4% specimen.[12]

Spectrum-imaging of the 50.7% specimen (Fig. 2) showed an increase in the Ti/Ba ratio at the grain boundaries, similar to our previous findings on the 53.4% film.[12] Compared to the grain interiors, all of the boundaries appear to be Ba deficient with *no* detectable increase in Ti content. The spatial resolution of the present analysis (determined primarily by the beam broadening) is about 5 nm, as can be deduced from the full width at half-maximum of the peaks in the line profiles of Ti/Ba ratio taken across the grain boundaries [Figs. 3(a) and 3(b)]. The effective thickness of a grain boundary varies from about 1 nm for the core (Fig. 1) to some larger value if space charge regions are included. Assuming a cylindrical shape for the analyzed volume, the numbers measured at the grain boundaries are related to the actual Ti/Ba ratios, $(Ti/Ba)_{GB}$, by a factor of $\pi d/4t$, where d is the diameter of the analyzed volume (~5 nm) and t is the grain boundary thickness. According to our measurements, the product $(Ti/Ba)_{GB} \times t$ is about 6 (with t in nm). No significant difference in the amount of segregation to the grain boundaries (excluding those with an amorphous phase) was observed between 50.7% and 53.4% specimens. For the amorphous pockets with a size

TABLE I. Chemical compositions of two BST films as measured by XRF.

	XRF	
Element	53.4% Specimen	50.7% Specimen
Ti	53.44 ± 0.22[a]	50.67 ± 0.22
Ba	33.21 ± 0.31	35.45 ± 0.31
Sr	13.35 ± 0.10	13.88 ± 0.1

[a]Compositions are given in at.% of the total metal fraction. Uncertainties correspond to a single standard deviation.

TABLE II. Cation ratios as measured by XRF and EELS.[a]

	53.4% Specimen		50.7% Specimen
Cation ratio	XRF	EELS	XRF
Ti/Ba	1.61 ± 0.02[a]	1.59 ± 0.08	1.43 ± 0.01
Ti/Sr	4.0 ± 0.03	3.94 ± 0.25	3.66 ± 0.03
Ba/Sr	2.49 ± 0.03	2.48 ± 0.19[b]	2.55 ± 0.03
Ti/(Ba + Sr)	1.15 ± 0.01	1.13 ± 0.07[b]	1.03 ± 0.01

[a]Uncertainties correspond to a single standard deviation.
[b]Calculated from Ti/Ba and Ti/Sr ratios.

of 2–3 nm, the Ti/Ba ratio in the pocket is estimated to be between 4 and 5 from the measured ratios of Ti/Ba [Fig. 3(c)] obtained with a 5-nm probe.

The average Ti/Ba ratios measured in the grain interiors are 1.29 ± 0.04 and 1.36 ± 0.05 for the 50.7% and 53.4% specimens, respectively. The uncertainties correspond to a single standard deviation as determined from 12 grains. Because the BST films studied have an average Ti/(Ba + Sr) ratio greater than unity, it is reasonable to assume that the grain interiors in these films are either stoichiometric or Ti rich. The Ti/Ba ratios inside the grains for both specimens were found to be reproducibly (three maps for each specimen) smaller than the values of 1.39 (50.7%) and 1.4 (53.4%) calculated for the case of Ti/(Ba + Sr) = 1 using mean values of Ba/Sr ratio measured by XRF (Table II). The difference is statistically significant for the film with 50.7%. These estimates suggest an inhomogeneous distribution of the Ba/Sr ratio in the specimen, with smaller values at the grain boundaries than in the grain interiors; however, the precision of the present EELS measurements is not sufficient to ascertain a dependence of the Ba/Sr ratio in the grain interiors on the overall composition.

For the 50.7% and 53.4% specimens, the average Ti/Ba ratio in the grain interiors is less than the overall Ti/Ba ratio (Table II). In addition, the Ba content was lower in the grain boundaries than in the grain interiors, whereas the Ti content remained approximately the same [Figs. 2(a) and 2(b)]. These combined results suggest that the [Ti/(Ba + Sr)] $\geqslant 1$ ratios in the specimens are accommodated by the creation of A = Ba,Sr cation vacancies which segregate to the grain boundary regions. An inhomogeneous distribution of the Ba/Sr ratio in the films can be attributed to differences in the energies of formation of the Ba and Sr vacancies. Segregation of the Ba/Sr vacancies to the grain boundaries creates negative space-charge regions which are expected to be compensated by the positively charged grain-boundary

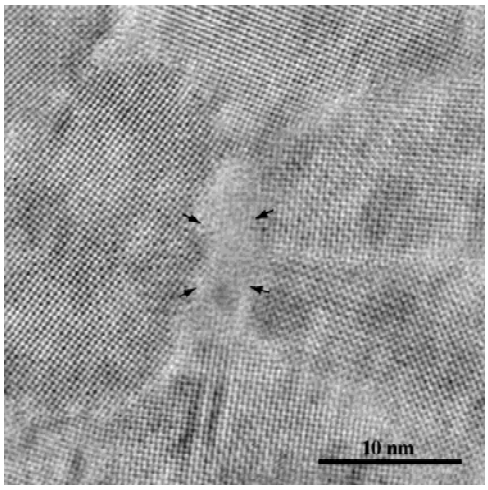

FIG. 1. HRTEM image of the BST film with 52% Ti (planar view). A region with amorphous-like contrast is indicated by the arrows.

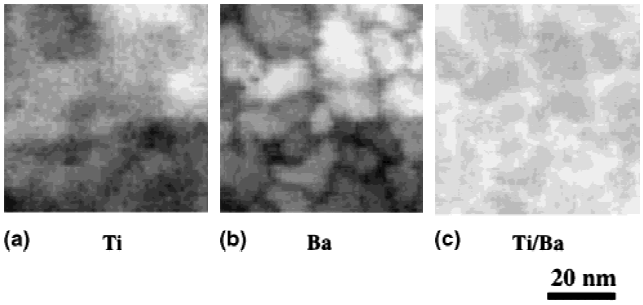

FIG. 2. Experimental maps of (a) Ti–$L_{2,3}$ and (b) Ba–$M_{4,5}$ absorbtion edge intensity distributions and (c) the calculated map of Ti/Ba ratio for the 50.7% film. Lighter contrast in the maps corresponds to a higher intensity of the corresponding absorbtion edges (or Ti/Ba ratio).

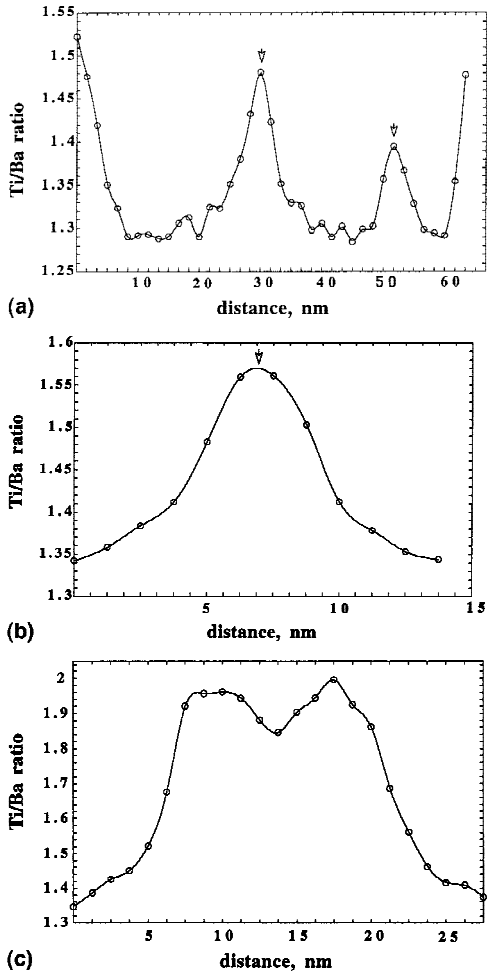

FIG. 3. Line profiles of Ti/Ba ratio across the grain boundaries in (a) the 50.7% and (b) the 53.4% specimens. The line profile for the 53.4% specimen was taken across a grain boundary free of amorphous phase. (c) Line profile across an amorphous region at a grain boundary junction in the 53.4% specimen. The grain boundaries are indicated by arrows. The dip observed in (c) has no significance.

cores.[16,17] This might be achieved either by an excess of Ti ions or by oxygen vacancies present at concentrations higher than those of the Ba/Sr vacancies;[16] in both cases an increased Ti/O ratio at the grain boundary core is expected. Surprisingly, measurements of the Ti/O ratio by Stemmer *et al.*[11] for a 50.7% film performed at much higher spatial resolution (a probe size of less than 0.4 nm has been quoted), did not reveal any visible change in Ti/O ratio at the grain boundaries. At present, there is no explanation for this discrepancy.

These results demonstrate that the BST films with Ti contents ranging from 50.7% to 53.4% consist of at least two phases with distinct chemical composition: grain interiors and grain boundaries. Assuming a hexagonal prism shape for grains with an average diameter of 15 nm, the volume fraction of grain boundaries with a thickness $t = 1$ nm is estimated to be 18%.[18] The grain boundaries in the present films are connected mostly in parallel to the grain interiors, and therefore their effect on the dielectric constant is expected to be roughly proportional to the volume fraction. Because the grain size is independent of the average composition, the grain boundaries alone cannot account for the strong compositional dependence of dielectric constant, even though the thickness of the space charge regions can vary with changes in the overall Ti/(Ba + Sr) ratio. As the Ti/(Ba + Sr) ratio is increased, a third, amorphous phase, containing Ba, Ti, O (and probably Sr) evolves at some of the grain boundaries and multiple grain junctions. Analysis of structural images suggests that the volume fraction of the amorphous phase increases from about 1% to 5–6% with an increase in the Ti content from 52% to 53.4%. No significant effects are expected for such small amounts of amorphous phase connected in parallel; however, this phase connected in series could strongly affect the dielectric constant. Because a large fraction of the amorphous phase is present in the form of pockets (see cross-sectional HRTEM images in Ref. 12), its contribution to the dielectric constant is expected to be between the two extreme cases. A possible effect of the amorphous phase can be estimated by assuming that the effective dielectric constant, ϵ_{eff}, of the BST films is represented by $\epsilon_{eff} = \frac{1}{2}(\epsilon_p + \epsilon_s)$ [$\epsilon_p = f_a\epsilon_a + (1 - f_a)\epsilon_c$ $(\epsilon_s)^{-1} = f_a(\epsilon_a)^{-1} + (1 - f_a)(\epsilon_c)^{-1}$, where ϵ_a and ϵ_c are dielectric permittivities of the amorphous and the crystalline phases, respectively, and f_a is a volume fraction of the amorphous phase], where ϵ_p and ϵ_s are dielectric permittivities calculated for the crystalline and the amorphous components connected in parallel and in sequence, respectively. Then, an amorphous phase with $\epsilon = 15$[19,20] and a volume fraction of 5% would reduce the effective dielectric constant from $\varepsilon = 280$[10] for the 50.7% specimen (no amorphous phase) to $\epsilon = 208$ for the 53.4% specimen. This value is still significantly larger than the $\epsilon = 160$ measured for the 53.4% specimen;[10] thus, there must be some additional factors contributing to the drop in permittivity. One such factor could be a dependence of the Ba/Sr ratio in the grain interiors on the overall Ti/(Ba + Sr) ratio in the film;[22] more precise measurements of the Sr content (i.e., Ti/Sr ratio) in the grain interiors are necessary to clarify this issue.

ACKNOWLEDGMENTS

The specimens for this study were kindly provided by P.C. van Buskirk, S. Bilodeau, and R. Carl of Advanced Technology Materials, Inc. The discussions with S.K. Streiffer (Argonne National Laboratory) are acknowledged. The use of brand or trade names does not imply endorsement of the product by NIST.

REFERENCES

1. T. Kawahara, M. Yamamuka, T. Makita, J. Naka, A. Yuuki, N. Mikami, and K. Ono, Jpn. J. Appl. Phys. **33,** 5129 (1994).
2. P.C. van Buskirk, J.F. Roeder, and S. Bilodeau, Integr. Ferroelectr. **10,** 9 (1995).
3. M. Yoshida, H. Yamaguchi, T. Sakuma, and Y. Miyasaka, J. Electrochem. Soc. **142,** 244 (1995).
4. T. Horikawa, N. Mikami, T. Makita, J. Tanimura, M. Kataoka, K. Sato, and M. Nunoshita, Jpn. J. Appl. Phys. **32,** 4126 (1993).
5. S. Yamamichi, J. Yabuta, T. Sakuma, Y. Miyasaka, Appl. Phys. Lett. **64,** 1644 (1994).
6. C.S. Hwang, S.O. Park, H-J. Cho, C.S. Kang, S.I. Lee, and M.Y. Lee, Appl. Phys. Lett. **67,** 2819 (1995).
7. J.S. Horwitz, W. Chang, A.C. Carter, J.M. Pond, S.W. Kirchoefer, D.B. Chrisey, J. Levy, and C. Hubert, Integrated Ferroelectrics **22,** 799 (1998).
8. A.I. Kingon, S.K. Streiffer, C. Basceri, and S.R. Summerfelt, MRS Bull. **21**(7), 46 (1996).
9. C. Basceri, S.E. Lash, C.B. Parker, S.K. Streiffer, A.I. Kingon, M. Grossman, S. Hoffman, M. Schumacher, R. Waser, S. Bilodeau, R. Carl, P.C. van Buskirk, and S.R. Summerfelt, in *Ferroelectric Thin Films VI,* edited by R.E. Treece, R.E. Jones, C.M. Foster, S.B. Desu, and I.K. Yoo (Mater. Res. Soc. Symp. Proc. **493,** Warrendale, PA, 1998), pp. 9–14.
10. S.K. Streiffer, C. Basceri, C.B. Parker, S.E. Lash, and A.I. Kingon, J. Appl. Phys. **86,** 4565 (1999).
11. S. Stemmer, S.K. Streiffer, N.D. Browning, and A.I. Kingon, Appl. Phys. Lett. **74,** 2432 (1999).
12. I. Levin, R.D. Leapman, D.L. Kaiser, P.C. van Buskirk, S. Bilodeau, and R. Carl, Appl. Phys. Lett. **75,** 1299 (1999).
13. P.C. van Buskirk, J.F. Roeder, and S. Bilodeau, Integr. Ferroelectr. **10,** 9 (1995).
14. S.M. Bilodeau, R. Carl, P.C. van Buskirk, J.F. Roeder, C. Basceri, S.E. Lash, C.B. Parker, S.K. Streiffer, and A.I. Kingon, J. Korean Phys. Soc. **32,** S1591 (1998).
15. R.D. Leapman and D.E. Newbury, Anal. Chem. **65,** 2409 (1993).
16. Y-M. Chiang and T. Takagi, J. Am. Ceram. Soc. **73,** 3278 (1990).
17. S.B. Desu and D.A. Payne, J. Am. Ceram. Soc. **73,** 3391 (1990).
18. R.T. DeHoff and F.N. Rhines, *Quantitative Microscopy* (McGraw-Hill, New York, 1968).
19. B.S. Chiou and M.C. Lin, Thin Solid Films **248,** 247 (1994).
20. Z.Q. Shi, Q.X. Jia, and W.A. Anderson, J. Vac. Sci. Technol. A, **10,** 733 (1992).
21. H. Funakubo, Y. Takeshima, D. Nagano, K. Shinozaki, and N. Mizutani, J. Mater. Res. **13,** 3512 (1998).